Title

PICOSECOND STUDIES OF THE TEMPERATURE DEPENDENCE OF HOMOGENEOUS AND INHOMOGENEOUS VIBRATIONAL LINEWIDTH BROADENING IN LIQUID ACETONITRILE

Authors

George, S.M.
Harris, A.L.
Berg, M.
et al.

Publication Date

1983-02-01

LBL-15641
Preprint

Lawrence Berkeley Laboratory
UNIVERSITY OF CALIFORNIA

Materials & Molecular Research Division

Submitted to the Journal of Chemical Physics

PICOSECOND STUDIES OF THE TEMPERATURE DEPENDENCE OF HOMOGENEOUS AND INHOMOGENEOUS VIBRATIONAL LINEWIDTH BROADENING IN LIQUID ACETONITRILE

S.M. George, A.L. Harris, M. Berg, and C.B. Harris

February 1983

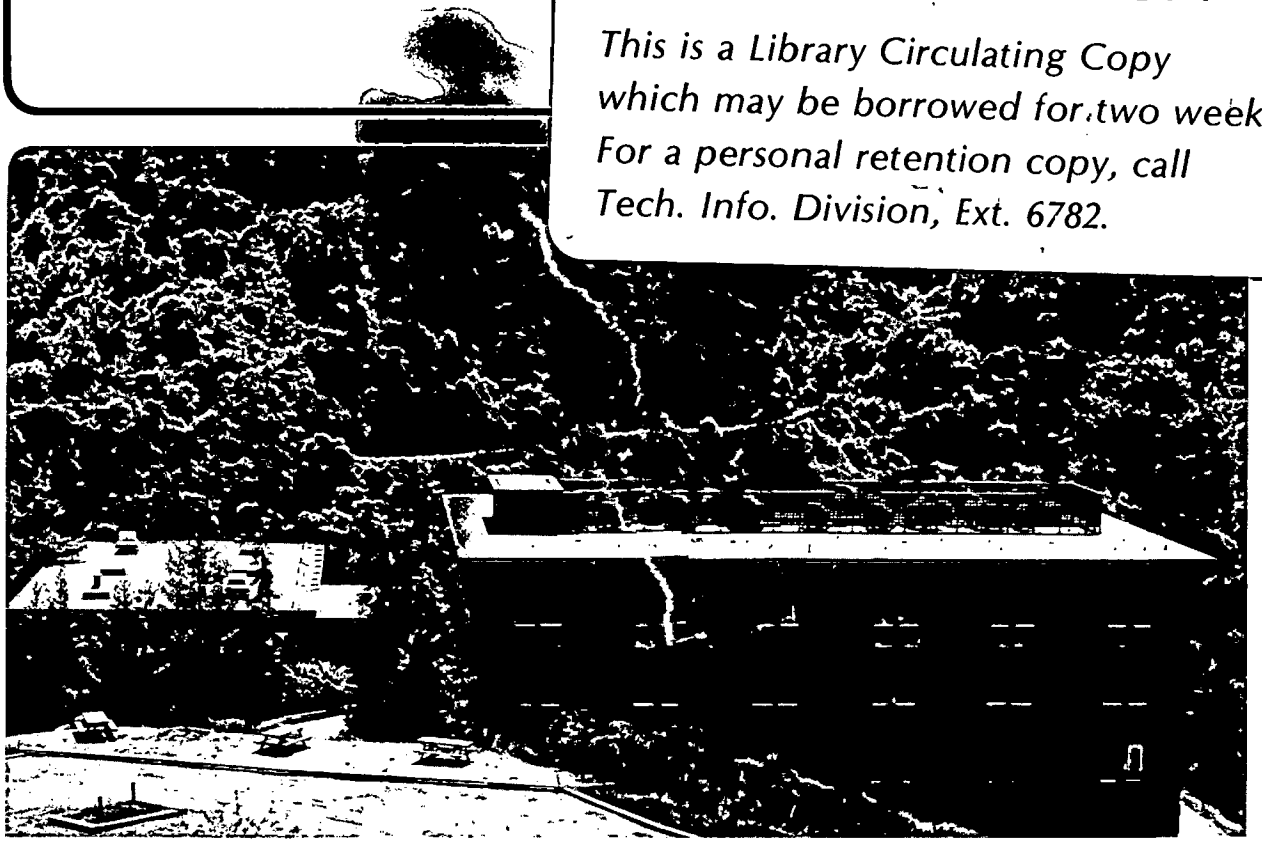

Prepared for the U.S. Department of Energy under Contract DE-AC03-76SF00098

DISCLAIMER

Picosecond Studies of the Temperature Dependence of Homogeneous and Inhomogeneous Vibrational Linewidth Broadening in Liquid Acetonitrile

S.M. George, A.L. Harris, M. Berg and C.B. Harris

Department of Chemistry and Materials and Molecular Research
Division of Lawrence Berkeley Laboratory
University of California, Berkeley, California 94720

Abstract

The temperature dependence of homogeneous and inhomogeneous vibrational linewidth broadening is reported for the symmetric CH_3-stretching vibration in acetonitrile over its entire liquid range at P=1 Atm. A selective excite-and-probe vibrational dephasing experiment based on transient stimulated Raman scattering in high laser depletion is used to measure the homogeneous dephasing times, T_2. The separation of homogeneous and inhomogeneous broadening processes is accomplished using the combined results of isotropic spontaneous Raman studies and selective picosecond vibrational dephasing experiments. As a function of temperature, the relative contributions of homogeneous and inhomogeneous broadening are shown to change significantly in opposing directions. Agreement between experiment and theory supports previous suggestions that homogeneous broadening is caused by rapidly varying processes which affect the vibration via short range repulsive forces. The results also suggest that inhomogeneous broadening is caused by slowly varying local density sites which interact with the vibration through long range attractive forces.

I. Introduction

Vibrational linewidths in liquids are broadened by many different mechanisms and experimental separation of the various mechanisms has been extremely difficult. Recently, selective picosecond vibrational dephasing experiments [1-5] have attempted to separate the broadening processes which act on rapidly and slowly varying timescales. The rapidly varying liquid processes are associated with homogeneous broadening, whereas the slowly varying processes are associated with inhomogeneous broadening. Recent theoretical work has placed this separation of timescales on firm theoretical foundations and has linked the slowly varying processes to attractive interactions in the liquid [6]. Previous work has already established a connection between rapidly varying liquid processes and repulsive interactions [7,8].

The vibrational linewidth broadening of the symmetric CH_3-stretching vibrational mode (ν_1) of acetonitrile has been studied extensively by isotropic Raman investigations [9-12]. Despite these investigations, the exact mechanism of vibrational linewidth broadening has remained elusive. Some studies have revealed that short range repulsive, collisional mechanisms may be dominant [9,10]. Other studies have emphasized the importance of the long range attractive dipole-dipole or dispersion broadening mechanisms [11,12]. Unfortunately, because isotropic Raman lineshapes can be both homogeneously and inhomogeneously broadened, isotropic Raman investigations can not separate the homogeneous and inhomogeneous vibrational linewidth broadening contributions. At the present date, only picosecond vibrational dephasing experiments combined with isotropic Raman investigations can separate these contributions.

In order to test the various homogeneous and inhomogeneous linewidth broadening mechanisms, we measured the temperature dependence of the picosecond dephasing times and isotropic Raman linewidths of the symmetric CH_3-stretching vibration in liquid acetonitrile over its entire liquid range from -40° to 70° C at P=1 Atm. [13]. The excite-and-probe vibrational dephasing experiments were conducted using a selective technique based on transient stimulated Raman scattering in high laser depletion [14]. This is the first picosecond examination of the temperature dependence of the homogeneous and inhomogeneous vibrational linewidth broadening in a liquid. The results demonstrate that both rapidly and slowly varying processes contribute to vibrational linewidth broadening.

II. Selectivity in Vibrational Dephasing Experiments

Vibrational dephasing experiments are performed with excitation pulses and time-delayed probe pulses [1]. Selectivity is the ability of the probing process to select out a single, distinct vibrational subgroup from a vibrational lineshape which is composed of a slowly varying frequency distribution of vibrational subgroups, i.e. inhomogeneously broadened. The higher the selectivity, the more accurately the decay of the probe scattering is related to the homogeneous dephasing time T_2 of a single vibrational subgroup.

We have recently developed a general theory for excite-and-probe vibrational dephasing experiments conducted using transient stimulated Raman scattering in low and high depletion of the excitation laser pulse [14]. The theory reveals that selectivity in the probing process of the vibrational dephasing experiment is very different in high and low laser depletion. Selectivity is low in low laser depletion. In marked contrast, high laser depletion produces a distinctive new behavior which leads to greatly enhanced selectivity. The results indicate that high laser depletion is necessary to measure the homogeneous vibrational dephasing time T_2 to a high level of accuracy in an inhomogeneously broadened vibrational linewidth [14].

Zinth et al. [15] have recently presented results from vibrational dephasing experiments conducted in low depletion of the excitation laser pulse. In agreement with theoretical interpretations [14,15], the measurements indicated that the excite-and-probe vibrational dephasing experiments conducted in low laser depletion were <u>not</u> selective. On the other hand, many previous excite-and-probe vibrational dephasing experiments by Kaiser and coworkers [1,2,16,17] and Harris and coworkers [3-5] have given

results which have displayed significant selectivity. These experiments were believed to have been conducted in low laser depletion. Consequently, these selective results [1-5,16,17] are in disagreement with the theoretical interpretation for vibrational dephasing experiments conducted in low laser depletion [14,15].

The previous experimental results [1-5,16,17] which have displayed selectivity are consistent with the high laser depletion results of the general theory [14]. Thus the discrepancies between these vibrational dephasing experiments and their theoretical interpretations can be explained if these excite-and-probe vibrational dephasing experiments were actually conducted in high laser depletion. This explanantion is highly probable because of the likelihood of high laser depletion in transient stimulated Raman scattering [14,18]. We note that our previous vibrational dephasing experiments [3-5] which have displayed significant selectivity are now known to have been undertaken in high laser depletion [18].

III. Experimental

Homogeneous linewidths were extracted from the symmetric CH_3-stretching vibrational linewidth in liquid acetonitrile using the selective excite-and-probe vibrational dephasing experiment based on high laser depletion of the excitation laser pulse and collinear coherent Stokes probe scattering [14]. The fundamentals of excite-and-probe vibrational dephasing experiments have been previously discussed [1,3,14]. Because of the discrepancies in recent picosecond vibrational dephasing studies [1-5,15-17], however, there is a great need to present explicit and thorough experimental details. Therefore, this section will discuss the many details and procedures which are important for accurate, reproducible experimental results.

A. Picosecond Pulse Generation

A schematic of the picosecond pulse generating system is shown in Fig. 1. The selective excite-and-probe vibrational dephasing experiments were performed with single picosecond pulses selected from the rising edge of pulse trains emitted by a TEM_{00} selective, passively mode-locked Nd:glass laser oscillator. The design, operation and performance of this laser have been given in thorough detail [19]. A Pockels cell driven by a low jitter electronic circuit [20] consistently selected the 4th-8th intense pulse from the rising edge of pulse trains of 30-45 pulses. A fast photodiode and a Tektronix 7834 fast storage oscilloscope monitered the pulse trains. Shots which displayed multiple pulse trains were excluded from the data. The selected pulse was amplified by two Nd:glass amplifiers. The pulse energy after amplification was determined to be approximately 1 mJ using a

Korad/Hadron Model 100 thermopile. Throughout this experiment, the pulse energy was kept essentially constant.

B. Pulse Characterization

In order to determine the width of the 1.06 μ pulse, the pulse autocorrelation widths were measured using two photon fluorescence (TPF). Unfortunately, the approximately 1 mJ 1.06 μ pulses used in this experiment were not intense enough for sufficient TPF signals. Higher pulse energies of approximately 20 mJ obtained using three Nd:glass amplifiers were required. Burn spots from these pulses on developed but unexposed Polaroid film taken before the TPF apparatus had diameters of 5-6 mm and showed no substructure.

The entire unfocused 1.06 μ pulse was sent into a standard TPF apparatus [21-23] shown in Fig. 1. The TPF signal was obtained from a 1×10^{-3} M methanol solution of rhodamine 6G in a 1 cm cell. An 85 mm camera lens imaged the TPF trace with a magnification of approximately 1.0 on a Princeton Applied Research (PAR) Model 1254 optical multichannel analyzer (OMA) ISIT detector. High f-numbers of f/22 to f/8 were used to maximize the depth of field. The OMA was interfaced to a minicomputer which displayed the TPF intensity plot on a CRT screen [24]. Calibration, focus and resolution of the lens-OMA system were determined using a calibrated copper mesh at the TPF cell position.

TPF peak-to-background ratios were in the range 2.8-3.0 to 1.0 on all shots. This indicates excellent pulse coherence. Autocorrelation widths of 1.69 ± 0.20 mm were obtained for pulses early in the rising edge of the pulse trains. This indicates that the pulses display small shot-to-shot pulse width fluctuations. Assuming pulse shapes intermediate between Gaussian and Lorentzian, the autocorrelation width corresponds to pulse widths of

≈9 psec [25]. Given the ≈400 micron mode-locking dye cell length in our Nd:glass laser oscillator [19], this measurement is in excellent agreement with previous studies of the 1.06 μ pulsewidth as a function of mode-locking dye cell length [26,27].

C. Pulse Compression and Frequency Doubling

Before frequency doubling, the 1.06 μ pulses were compressed using a saturable absorber [28]. The saturable absorber, Eastman Kodak dye #9860, was dissolved in 1,2-dichloroethane in a 1 cm cell until an optical density of 1.0 was measured at 1.06 μ. The cell was placed after the final ampliflier as shown in Fig. 1. The dye absorbs the rising edge of the 1.06 μ pulse, then bleaches, allowing the main portion of the pulse to pass. Using this saturable absorber, our excite-and-probe vibrational dephasing experiments have measured coherent Stokes signal decays as rapid as $T_2/2$≈0.5–0.7 psec in dimethylsulfoxide in agreement with previous measurements [3]. This indicates that the rising edge of the pulse is <0.5–0.7 psec. This rapid rising edge is important for adequate time resolution in this experiment.

The effect of the saturable absorber on the 1.06 μ pulse width was also investigated using the TPF apparatus. The effect of the saturable absorber on pulses of approximately 20 mJ was studied. The average measured pulse shortening ratios were 0.89 and 0.80 at optical densities of 1.0 and 2.0, respectively [29]. These pulse shortening ratios are based on the average of 20–30 individual shots at each optical density. Smaller ratios are expected for the ≈1 mJ pulses used in the experiment. In addition, the saturable absorber did not significantly broaden the pulse's spectral bandwidth. Spectral examinations of the frequency doubled 5306 Å pulse revealed that the

compressed pulse spectrum was broadened by <10 % relative to an uncompressed pulse.

The compressed pulses were centered into a KDP angle-tuned doubling crystal and the crystal was adjusted for maximum doubling effeciency by monitoring both the incident 1.06 μ pulse and the transmitted 5306 Å pulse. The spatial profile of the transmitted 5306 Å pulse was very sensitive to the crystal angle. When the crystal was set at the maximum doubling efficiency, the spatial profile was round and clean with no substructure. Before each experimental run, the doubling crystal was adjusted for optimum efficiency and the quality of the spatial profiles was monitored. We observed that stimulated Raman excitation occured at much lower energy thresholds when the pulse had high quality spatial profiles.

Spectral examinations of these 5306 Å pulses using the PAR Model 1254 OMA ISIT detector displayed spectral bandwidths (FWHM) of 5.0±1.2 cm^{-1}. Assuming pulse shortening in the saturable absorber and in the KDP crystal, pulsewidths of approximately 6-8 psec were estimated for the 5306 Å pulses. The resultant bandwidth product of ≈0.9 indicates that the pulses were essentially bandwidth limited.

D. Optics Alignment and Experimental Adjustments

The selective, picosecond Stokes scattering technique is dependent upon collinear overlap of the excite and probe pulses to assure selectivity [14]. In order to easily align the optics for proper overlap, a Helium-neon laser beam was aligned collinear to the Helium-neon laser beam which was used to align the Nd:glass laser oscillator. This was accomplished using a

translatable pellicle shown in Figs. 1 and 2. Using this brighter second beam, the optics could be easily aligned.

The excitation and probe telescopes were both adjusted for focal lengths at the center of the 10 cm acetonitrile [30] Raman cell shown in Fig. 2. The beams were collinearly overlapped by xy adjustments of the convex lens on the excite and probe line telescopes and by xy adjustments of the two mirrors in the probe line. Before each experimental run, the overlap was carefully checked at the first Glan-laser polarizer, at the 10 cm acetonitrile cell and at the second Glan-laser polarizer with both the Helium-neon alignment beam and the 5306 Å pulses.

The minimum divergence, α, of the excitation Stokes pulse with respect to the axis of the excitation laser pulse is important for reproducible results and minimum depolarization in the second Glan-laser polarizer. Before each experimental run, the stimulated Stokes divergence was monitored and the intensity of the excitation laser pulse was adjusted for the minimum Stokes divergence which occurs for a narrow range of laser pulse energies just above the stimulated Raman threshold. Assuming a point source at the center of the Raman cell shown in Fig. 2, cones of stimulated Stokes light with α=3-10 mrad were observed at the second Glan-laser polarizer for laser excitation pulses within this narrow energy range of acceptable data shots. Shots of greater energy could generate cones of stimulated Stokes with α>15 mrad.

F. Optical Detection and Data Selection

The stimulated Stokes excitation pulse and the coherent Stokes probe pulse are collinear and their separation relies upon their perpendicular polarizations. Because the excitation Stokes pulse is much larger than the

probe Stokes pulse, depolarization of the excitation Stokes pulse in the crossed Glan-laser polarizers or in the 10 cm Raman cell can completely overwhelm the coherent probe Stokes signal. For this reason, high quality, polarizers with extinctions of approximately 1×10^{-6} were used [31]. The temperature-controlled Raman cell is discussed in Sec. IV.

As shown in Fig. 2, the excitation Stokes pulse and the coherently scattered probe Stokes pulse were separated by the second Glan-laser polarizer because of their different polarizations. They were spatially separated on the slits of a Spex 3/4 m monochromator and were simultaneously detected, but spatially resolved, on the target of a two-dimensional optical multichannel analyzer. This analyzer is interfaced to a minicomputer which displayed and integrated the spectral line shapes of the excite and probe Stokes pulses [24].

The stimulated Stokes spectrum (FWHM) determined from laser shots within the acceptable range was 16 ± 7 cm^{-1}. Laser shots of greater energy generated much broader, very random excitation Stokes spectra. We spectrally observed each shot and discarded any shot which displayed significant frequency modulation. The transmitted excitation laser pulse spectrum (FWHM) determined from laser shots within the acceptable range was 8.3 ± 2.8 cm^{-1}, broadened considerably from the incident excitation laser pulse spectrum (FWHM) of 5.0 ± 1.2 cm^{-1}. This broadening of the transmitted excitation laser pulse spectrum is consistent with the shortening of the excitation laser pulse in high laser depletion [14].

Before signals were calculated, the coherent probe Stokes signal was corrected for excitation Stokes signal depolarization. Probe Stokes signals were measured as a function of excitation Stokes energy with the laser probe pulse blocked. Within a certain range of excitation laser pulse energies and

excitation Stokes pulse energies, this depolarization was very linear. At higher excitation energies, the deplorization became large and unpredictable. This point was approximately where the Stokes divergence became large and where the Stokes spectrum began to modulate. Shots above this level were excluded from the data.

Shots which showed very low Stokes conversion from lower energy laser excitation pulses also displayed significant scatter in the probe signal. This scatter may reflect the selectivity differences in high and low laser depletion [14]. These low Stokes conversion shots were also excluded from the data. Only shots within the restricted range shown in Fig. 3 were accepted. Shots within this narrow window displayed some scatter, but the scatter did not correlate with the excitation pulse energy.

G. Excitation Laser Pulse Depletion

In order to characterize the laser pulse depletion in this experiment, we measured the excitation laser pulse depletion in the 10 cm acetonitrile Raman cell. Figure 3 shows the transmitted laser pulse energy versus the incident laser pulse energy at 5306 Å with and without the 10 cm Raman cell. The approximate range of laser pulse energies used in the experiment is also given.

Figure 3 shows that immediately after the stimulated Raman scattering threshold is reached, the laser can be depleted >10% and depletion approaches ≈50% as the incident laser energy increases. In other studies [18], we measured both transmitted laser and Stokes pulse energies after the Raman cell as a function of incident laser pulse energy. Coincident sharp thresholds for stimulated Stokes scattering and subsequent laser depletion versus incident

laser pulse energy were observed. There was a nearly one-to-one relationship between photons removed from the transmitted laser pulse and photons added to the transmitted Stokes pulse. Consequently, we are confident that this vibrational dephasing experiment was performed with excitation pulses in the high laser depletion regime.

IV. Temperature-Controlled Cell

In order to minimize depolarization in the 10 cm Raman cell, the temperature-controlled cell shown in Fig. 4 was designed. Birefringence in the windows of the cell was the major difficulty and low birefringence glass windows were required. Schott glass SF-57 was selected because of its extremely low birefringence. Unfortunately, SF-57 is a soft, high density lead glass and is difficult to polish. Using the proper polishing techniques, the 2 mm thick SF-57 glass flats used in this experiment were polished optically flat ($\approx\lambda/2$) with nearly parallel surfaces. After polishing and between experimental runs, the windows were stored in a dessicator. This precaution was taken because the SF-57 glass surface is sensitive to water and other chemicals.

The birefringence problem was complicated by the different thermal expansion coefficients of the various materials in the cell. A strain relieving copper window mount identical to the design presented by Mollenauer et al. [32] was used to eliminate the thermally-induced strain birefringence. We had difficulties with their epoxy recipe because the curing cycle at 150° C caused the SF-57 glass to be chemically etched. We resorted to a 50-50 mixture of Shell Epon Resin 828 and Versamid 140 polyamide resin [33]. This epoxy mixture cures at room temperature in approximately 48 hours

and gives a flexible, leak-tight and temperature resistent seal. The window mounts were attached to the copper low temperature cell using a retaining ring which was screwed down around the copper window mount and allowed the windows to be taken on and off easily. A flat teflon ring formed the seal between the window mount and the copper low temperature cell.

An additional special design was employed for the -40° C and -10° C temperature points. This design involved flowing nitrogen gas through a series of baffles [34]. A vertical cross section of the temperature regulating cell utilyzing this design is shown in Fig. 4. Using the "gas windows", the temperature gradient between the windows of the 10 cm cell and room temperature was accepted by the outwardly flowing dry nitrogen gas and the flowing gas prevented water vapor from condensing on the windows. As a result, the "gas window" design avoided the necessitity of using two additional outside windows and a vacuum jacket. During experimental runs, nitrogen gas flow rates of approximately 1 liter per minute were used for each window. More vigorous flow rates are were used to flush out the system prior to cooling the low temperature cell.

When controlling the cell at -40°, -10°, 45° and 70° C, the temperature cell was insulated with styrofoam. The temperature of the cell was regulated at 70°, 45° and -10° C using a Lauda K-2/R circulator. The temperature was controlled at -40° C using a dry ice/o-xylene/m-xylene slush bath [35] to control the circulating coolant temperature. The cell temperature was monitered using a copper/constantan thermocouple mounted on the copper block of the cell.

V. Results

Some representative normalized coherent Stokes signals versus delay time at the various temperatures are shown in Figs. 5(a) and 5(c) and Figs. 6(a) and 6(c). Each point in the slope region of these vibrational dephasing curves is an arithmetic average of approximately 10-25 individual shots. The error bars represent the standard deviation of the individual coherent Stokes signals. If the standard deviation of the mean was used, the calculated error bars were less because of the large number of individual shots. The error bars associated with the standard deviation of the mean led to an accuracy of ±0.2 psec in the slope measurement.

The central point average [36] indicated by the open triangles is also shown in the slope region of Figs. 5(a) and 5(c) and Figs. 6(a) and 6(c). Close agreement of the arithmetic average and the central point average illustrates that the pulse durations are not fluctuating significantly. This is in agreement with the TPF investigations in Sec. III.B.

The experimental dephasing times from individual measurements are shown in Fig. 7. The measurements are numbered according to the sequence in which they were performed. Figure 7 illustrates that the decay times from individual measurements at the various temperatures are consistently different and reproducible. The experimental error of ±0.2 psec on the individual $T_2/2$ measurements is well within the differences between various temperatures.

Recent theoretical studies have indicated that non-selective behavior is expected in low laser depletion [14,15]. On the other hand, our general theory has revealed that high laser depletion leads to enhanced selectivity which enables homogeneous dephasing time T_2 to be measured to a high level of accuracy in inhomogeneously broadened vibrational linewidths [14]. We note

that if this high laser depletion experiment was not selective, the probing process should have yielded nearly identical rapid coherent Stokes signal decay curves at each temperature [14,15]. This predicted non-selective behavior corresponds to the nearly invariant temperature-dependent isotropic Raman linewidth of the symmetric CH_3-stretching vibration in liquid acetonitrile [11]. Figure 7 demonstrates that this behavior was not observed. Thus the different, reproducible vibrational dephasing times measured using high laser depletion support the results of our general theory [14].

The level of accuracy of the T_2 measurement in high laser depletion has been previously discussed [14]. In this experiment, we estimate that the measured decay time is approximately >80-90% of the actual $T_2/2$ homogeneous decay time. Because of this high level of accuracy, we assumed that the experimentally measured decay is equivalent to $T_2/2$ in the following analysis.

The isotropic spontaneous Raman lineshapes at the various temperatures are shown in Figs. 5(b) and 5(d) and Figs. 6(b) and 6(d). The homogeneous linewidths $\Delta\omega_H$ (FWHM) of the Lorentzian lineshapes corresponding to the average measured homogeneous dephasing times, $T_2/2$, were calculated using:

$$\Delta\omega_H(cm^{-1}) = 1/c\pi T_2 \qquad (1)$$

The homogeneous Lorentzian lineshapes are drawn in Figs. 5(b) and 5(d) and Figs. 6(b) and 6(d). From these superimposed lineshapes, the inhomogeneous broadening can easily be visualized.

The inhomogeneous broadened linewidths were calculated by deconvoluting the homogeneous lineshapes from the spontaneous Raman lineshapes. The deconvolution method assumed a Lorentzian homogeneous lineshape and a Gaussian

inhomogeneous lineshape and has been previously discussed [3]. The average experimental $T_2/2$ times, the calculated homogeneous linewidths(FWHM), the measured isotropic Raman spontaneous linewidths(FWHM) and the calculated Gaussian inhomogeneous linewidths(FWHM) are given in Table 1.

VI. Temperature Dependent Vibrational Linewidth Broadening

A. Homogeneous Broadening

Many homogeneous linewidth broadening mechanisms have been proposed [8]. The binary collision [7], the hydrodynamic [37], and the Lynden-Bell [38] models assume that pure dephasing mechanisms predominate and are frequently employed because their predictions are made in terms of measurable physical parameters. For example, predicted homogeneous linewidths are proportional to: $\eta T/\rho$ for the binary collision model; ηT for the hydrodynamic model; and $\rho\eta/T$ for the Lynden-Bell model where ρ is the liquid number density, η is the viscosity and T is the temperature.

Figure 8(a) shows the temperature dependence of the correlation between the homogeneous linewidths calculated from the measured dephasing times using Eq. (1) and the predicted homogeneous linewidths. The predicted theoretical values were calculated using measured density [39-43] and viscosity [40,41,43,44] values. The predicted homogeneous linewidths were normalized to give the experimentally determined homogeneous linewidth at 18° C.

The homogeneous broadening models correctly predict broader homogeneous linewidths at lower temperatures. The broader predicted linewidths are largely due to higher viscosity at lower temperatures. Assuming a collisional mechanism in which a collision perturbs the frequency of the vibration, the

higher viscosity indicates a higher repulsive collision rate which increases the homogeneous linewidth. The data at lower temperatures do not support one theory more than the others. None of these theories can account for the increased homogeneous linewidth above 45° C. This deviation at higher temperatures will be discussed in Sec. VII.

B. Inhomogeneous Broadening

Using picosecond excite-and-probe vibrational dephasing experiments which are now known to have been conducted using transient stimulated Raman scattering in high laser depletion, George, Auweter and Harris [3] measured dephasing times for symmetric CH_3-stretching vibrations in a variety of liquids. In conjunction with isotropic Raman studies, they showed that the vibrational linewidths for symmetric CH_3-stretching vibrations in nonhydrogen-bonded liquids at room temperature were inhomogeneously broadened to various degrees. A correlation was observed between the inhomogeneous broadening and the width of the number density distribution in the liquid [3]. The correlation suggested that a distribution of different, slowly varying, local number densities in a liquid creates a distribution of distinct vibrational frequencies.

Schweizer and Chandler (SC) have recently proposed a comprehensive vibrational dephasing theory. Their theory places the correlation between inhomogeneous broadening and the width of the local number density distribution in a liquid on firm theoretical grounds. Furthermore, their theory shows that long range attractive forces provide the coupling between the slowly varying local number density and the vibration [6].

When the attractive force correlation time, $T_A = \infty$, the SC theory leads to

the prediction that $\Delta\omega_{INH}$, the absolute inhomogeneous broadening linewidth (FWHM) is given by:

$$\Delta\omega_{INH} = 2(2\ln 2)^{1/2}/(N)^{1/2} \; X \; \langle\Omega_A\rangle(\rho \; k_B T \; \kappa_T)^{1/2} \qquad (2)$$

where ρ is the number density, $k_B T$ is the thermal energy, κ_T is the isothermal compressibility, N is the estimated average number of nearest neighbors and $\langle\Omega_A\rangle$ is the attractive force contribution to the gas-to-liquid frequency shift. Using this expression, SC [6] found that their predictions were in agreement with isothermal density dependent isotropic Raman linewidths in isobutylene [45]. In addition, the correlation between the predicted and measured inhomogeneous broadening linewidths observed by George, Auweter and Harris [3] was recently shown to be improved by the inclusion of the attractive forces in the SC theory [46].

The SC absolute inhomogeneous broadening linewidth is dependent on κ_T, the isothermal compressibility. Temperature-dependent isothermal compressibility values for acetonitrile were calculated from experimental PVT data [47] using the Tait equation [48]. In order to obtain κ_T values for temperatures outside of the measured range, a hard sphere isothermal compressibility model [49] was fit to the experimental values using σ= 4.27 Å at -40° C and $d\sigma/dT = -0.4 \; \Omega \; 10^{-3}$/deg where σ is the hard sphere diameter. These parameters are close to the values derived by Jonas et al. [9]. The temperature dependent heat of vaporization values used in the hard sphere model were calculated from heat capacity data [50]. The hard sphere model's fit to the experimental values is shown in Fig. 9.

The SC absolute inhomogeneous linewidth is also dependent on $\langle\Omega_A\rangle$, the attractive force contribution to the gas-to-liquid shift. Temperature-

dependent $\langle\Omega_A\rangle$ values for the symmetric CH_3-stretching vibration in acetonitrile were calculated according to the SC theory as previously described [46]. For consistency with the hard sphere model of isothermal compressibility, σ=4.27 Å at -40° C and $d\sigma/dT$=-0.4 X 10^{-3}Å/deg were used to evaluate the temperature-dependent cavity distribution function [6]. In addition, the small observed temperature-dependent vibrational frequency shift of =1.3 X $10^{-2}cm^{-1}$/deg was used to evaluate the experimental gas-to-liquid vibrational frequency shift [6]. Resultant $\langle\Omega_A\rangle$ values were -29.3, -28.6, -27.6, -26.8 and -25.8 cm^{-1} at -40°, -10°, 18°, 45° and 70° C.

Figure 8(b) shows the SC absolute inhomogeneous linewidths, $\Delta\omega_{INH}$, calculated according to Eq. (2) for three different representative N values [6]. These absolute predictions, based on $T_A=\infty$, are remarkably close to the experimentally determined inhomogeneous linewidths. Below 45° C, the SC theory correctly predicts broader inhomogeneous linewidths at higher temperatures. The temperature dependence of the inhomogeneous linewidth is determined largely by $(\kappa_T)^{1/2}$. Consequently, the higher liquid compressibility at higher temperatures increases the predicted absolute inhomogeneous linewidths. Above 45° C, the measured inhomogeneous linewidths are narrowed in comparison to the theoretical predictions. This deviation at higher temperatures will be discussed in Sec. VII.

C. Conclusions

These results demonstrate that homogeneous and inhomogeneous broadening contributions change significantly with temperature. Figures 8(a) and 8(b) reveal that the variations in the homogeneous and inhomogeneous linewidth broadening with temperature have opposing effects. Below 45° C, the

homogeneous linewidth decreases and the inhomogeneous linewidth increases with increasing temperature. In the case of acetonitrile, these counterbalancing homogeneous and inhomogeneous temperature dependences lead to little observed change in the isotropic Raman linewidth [11]. We note that these opposing temperature trends are predicted by the Schweizer-Chandler vibrational dephasing theory [6].

The agreement between experiment and theory supports the association of homogeneous broadening with rapidly varying short range processes. These rapidly varying processes, e.g., collisions, probably affect the vibration through repulsive forces. Likewise, the results support the association of inhomogeneous broadening with a distribution of slowly varying local number density sites. These local density sites are thought to interact with the vibration through the long range attractive forces in the liquid.

VII. Deviation from Theory at High Temperatures

Experimental [3] and theoretical [6] results suggest that a distribution of local density sites creates an inhomogeneous distribution of distinct vibrational frequencies through attractive force interactions. The lifetime of these local density sites determines the degree of separation between homogeneous and inhomogeneous broadening processes. When the lifetime is long, e.g., >10 psec, there is a clear separation. As the lifetime becomes shorter, the separation becomes less distinct and the inhomogeneous processes become homogeneous processes as previously discussed [3].

The local density sites are expected to persist for a lifetime approximately equal to the time necessary for a molecule to travel the range of the local density perturbation. Consequently, the lifetime of the local density sites is expected to be proportional to 1/D where D is the translational diffusion constant. The temperature-dependent translational self-diffusion constants in acetonitrile are obtained from NMR spin-echo measurements [51,52] and are shown in Fig. 10.

In the Schweizer-Chandler theory, the correlation time of the attractive force interactions, T_A, characterizes the lifetime of the various local density sites which give rise to inhomogeneous broadening through attractive force interactions. As expected, T_A is proportional to 1/D. Actual values of T_A are calculated in the Schweizer-Chandler theory by:

$$T_A > \sigma^2/(\pi^2 D) \qquad (3)$$

where σ is the hard core diameter [6]. When the temperature is low and the translational diffusion constant is small, Eqn. (3) predicts that T_A or the

lifetime of the local density sites is long. Consequently, the selective excite-and-probe vibrational dephasing experiment can measure the homogeneous linewidth of a single, distinct vibrational isochromat corresponding to a single local density site. Likewise, when the temperature is high and the translational diffusion constant is large, Eqn. (3) predicts that the lifetime of the local density sites is shorter.

Because the various local density sites form a closed set, a short lifetime for a local density site is equivalent to a rapid rate of interconversion or exchange between the various sites. The faster rate of site exchange at higher temperatures would have two effects: First, the inhomogeneous distribution of local density sites would be reduced by motional narrowing. Second, the homogeneous linewidth would be broadened by dephasing resulting from exchange between sites with different frequencies. Motional narrowing could account for the narrowing of measured inhomogeneous linewidths in comparison to theoretical predictions at higher temperatures shown on Fig. 8(b). Likewise, site exchange dephasing could account for the broadening of measured homogeneous linewidths in comparison to theoretical predictions at higher temperatures shown on Fig. 8(a).

The homogeneous linewidth broadening from site exchange would depend on the exact nature of the site exchange. Assuming two separate isochromats undergoing exchange in the Markov limit, the individual linewidths would broaden as $1/\tau$ where τ is the exchange time [53]. Consequently, as a simple extension of two-site exchange, the effect of diffusional site exchange on the homogeneous dephasing time T_2 was modeled according to:

$$2/T_2 = 2/T_2^* + 1/\tau \qquad (4)$$

where T_2^* is the pure dephasing time and τ is proportional to 1/D. Notice that the effect of τ on T_2 is similar to the effect of T_1, the population lifetime, on T_2 [7].

A fit to the data when τ = 4 psec at 70° C and T_2^* is based on the hydrodynamic dephasing model [37] is shown in Fig. 11. Figure 11 shows that the predicted $T_2/2$ times including diffusional site exchange display the correct qualitative behavior. We note that a τ= 4 psec at 70° C is in approximate agreement with the calculated $T_A > 2.3$ psec calculated from the Schweizer-Chandler theory using Eq. (3) with σ = 4.3 Å and D = 8.3×10^{-5} cm^2/sec. We believe that these results are consistent with the first observation of the interconversion of local density sites or "spectral diffusion" in a liquid.

VIII. Alternative Broadening Mechanisms

A. Other Possible Homogeneous Broadening Mechanisms

Many diverse mechanisms may influence the T_2 homogeneous dephasing time [8]. Ignoring the dephasing contribution from site exchange discussed in Sec. VII, the major T_2 dephasing contributions in liquids are generally believed to be: the pure dephasing time, T_2^*; the resonant energy transfer time, T_r; and the population relaxation time, T_1. In certain limits, the T_2 dephasing time can be expressed as [8]:

$$2/T_2 = 2/T_2^* + 2/T_r + 1/T_1 \qquad (5)$$

Isotope dilution studies indicate little contribution to T_2 from resonant

vibrational energy transfer [9,11]. In addition, the population lifetime is generally assumed to be much longer that T_2^*. If this assumption is valid, Eqn. (5) indicates that $T_2 \approx T_2^*$. This assumption was utilized in Sec. VI.A. On the other hand, recent experimental measurements have revealed that T_1 for the symmetric CH_3-stretching vibration in liquids can be extremely rapid [54,55]. Consequently, T_1 effects can make a significant contribution to T_2 and an analysis of the vibrational dephasing mechanisms must include possible population relaxation effects.

The rapid T_1 population relaxation times for the symmetric CH_3-stretching vibration are believed to be determined by the Fermi resonance between the symmetric CH_3-stretching vibration and overtones of the CH_3-bend [54-56]. Although T_1 has not been measured for acetonitrile, there are several indications which suggest that acetonitrile may have a Fermi resonance. Using the intensity method of determining Fermi resonance [57], a Fermi resonance would be predicted in acetonitrile between the symmetric CH_3-stretching vibration and the overtone of the symmetic CH_3-bending mode [58]. In addition, comparison of CH-stretching frequencies in CH_3CN and CHD_2CN provides a means to assess the Fermi resonance frequency shift [57]. Using this method, a positive Fermi resonance shift is determined [59].

The above evidence suggests that T_1 effects may make a contribution to the observed T_2 dephasing times. We note that, although our analysis of T_2 was performed assuming that $T_2^* \approx T_2$, a T_2 dominated by T_1 should have approximately the same temperature dependence. For example, in the binary collision model [7], T_1 depends directly on the collision rate and shows roughly the same dependence on macroscopic liquid parameters as T_2^*.

B. Other Possible Inhomogeneous Broadening Mechanisms

In addition to the inhomogeneous broadening mechanism based on slowly varying local density fluctuations, other slowly varying attractive or repulsive mechanisms may also establish various local sites in liquid acetonitrile and lead to inhomogeneous broadening. For example, the large electric dipole moment of acetonitrile can lead to dipole-dipole associativity. Thermodynamic investigations have emphasized the importance of dipole-dipole associativity [60-62]. Spectroscopic studies also have indicated the formation of dipole pairs or dipole-dipole complexes [63-67]. On the other hand, theoretical investigations have shown that hard core repulsive forces create clusters of orientational correlation in liquid acetonitrile [68]. Whatever the exact mechanism, X-ray and neutron scattering investivations have revealed the existence of correlation clusters in liquid acetonitrile with a diameter ≈11Å [69,70].

The existence of dipole-dipole associativity and correlation clusters in liquid acetonitrile suggests that a distribution of various slowly-varying dipole-dipole complexes or correlation clusters could create an inhomogeneous distribution of distinct vibrational frequencies. The distribution width of the various correlation clusters may be determined by the distribution width of the local number densities. Consequently, the temperature dependence of this inhomogeneous broadening would be expected to be similar to the predicted inhomogeneous broadening discussed in Sec. VI.B. In a similar manner to the local density sites discussed in Sec. VII, the lifetime of the correlation clusters would also be expected to be proportional to 1/D, where D is the translational diffusion constant. As a result, the deviation of the measured homogeneous and inhomogeneous linewidths from the theoretical predictions at

high temperatures could also be explained using this inhomogeneous broadening mechanism.

IX. Summary

The temperature dependence of homogeneous and inhomogeneous vibrational linewidth broadening is presented for the symmetric CH_3-stretching vibration in liquid acetonitrile from -40° to 70° C at P=1 Atm. The separation of homogenoeus and inhomogeneous broadening is accomplished using the combined results of isotropic spontaneous Raman studies and selective excite-and-probe vibrational dephasing experiments. The results show that homogeneous and inhomogeneous vibrational linewidth broadening contributions change in opposing directions with temperature.

At lower temperatures, the homogeneous linewidth decreases and the inhomogeneous linewidth increases with increasing temperature. The qualitative agreement between the measured homogeneous linewidths and the pure dephasing models supports previous suggestions that homogeneous broadening is caused by rapidly varying repulsive forces. The nearly quantitative agreement between the measured inhomogeneous linewidths and the absolute inhomogeneous linewidths predicted by the Schweizer-Chandler theory supports the suggestion that inhomogeneous broadening is caused by slowly varying attractive forces.

Inhomogeneous broadening contributes a substantial fraction to the symmetric CH_3-stretching linewidth in liquid acetonitrile. The temperature-dependent inhomogeneous broadening results supports the idea that a distribution of local number densities in the liquid creates an inhomogeneous distribution of distinct vibrational frequencies. At higher temperatures, the lifetime of the local number density sites affects the separation of

homogeneous and inhomogeneous broadening processes. The results are consistent with the first observation of the interconversion of local density sites or "spectral diffusion" in a liquid.

Different, reproducible vibrational dephasing times are measured at various temperatures using a technique based on transient stimulated Raman scattering in high laser depletion. This work supports the conclusions of a recent theory for selective vibrational dephasing experiments in high laser depletion [14]. The results indicate that, contrary to the work in low laser depletion [15], selective excite-and-probe experiments are possible in high laser depletion. Previous vibrational dephasing experiments [1-5,16,17] which are in conflict with the low laser depletion theory [14,15] can be explained if they were conducted in high laser depletion.

Acknowledgements

This work was supported by the National Science Foundation. In addition, some of the equipment utilized in this work was made possible by the Director, Office of Energy Research, Office of Basic Energy Sciences, Chemical Sciences Division of the U.S. Department of Energy under Contract Number DE-AC03-76SF00098. ALH and MB gratefully acknowledge the National Science Foundation for graduate fellowships. The authors thank S.J. Davis for his design and help in the construction of the low jitter electronic pulse selector. The authors also thank R.G. Snyder and V.L. Shannon for their measurements of the temperature dependent isotropic Raman linewidths. In addition, the authors are grateful to A. Wurflinger for sending the temperature dependent isothermal compressibility values for acetonitrile and to G. Williams and M.S. Beevers for suggesting the temperature regulated cell design. The authors also appreciate many useful discussions with K.S. Schweizer and L.R. Pratt.

References

1. A. Laubereau and W. Kaiser, Rev. Mod. Phys. 50, 607(1978).
2. A. Laubereau, G. Wochner and W. Kaiser, Chem. Phys. 28, 363(1978).
3. S.M. George, H. Auweter and C.B. Harris, J. Chem. Phys. 73, 5573(1980).
4. C.B. Harris, H. Auweter and S.M George, Phy. Rev. Lett. 44, 737(1980).
5. C.B. Harris, H. Auweter and S.M. George, in Picosecond Phenomena II, ed. by R.M. Hochstrasser, W. Kaiser and C.V. Shank, Springer Ser. Chem. Phys. 14 (Springer-Verlag, Berlin, Heidelberg, New York, 1980) p. 151.
6. K.S. Schweizer and D. Chandler, J. Chem. Phys. 76, 2296(1982).
7. S.F. Fischer and A. Laubereau, Chem. Phys. Lett. 35, 6(1975).
8. D.W. Oxtoby, Adv. Chem. Phys. 40, 1(1979).
9. J. Schroeder, V.H. Schiemann, P.T. Sharko and J. Jonas J. Chem. Phys. 66, 3215(1977).
10. K. Tanabe, Chem. Phys. 38, 125(1979).
11. J. Yarwood, R. Arndt and G. Doge, Chem. Phys. 25, 387(1977).
12. J. Yarwood, R. Ackroyd, K.E. Arnold, G. Doge and R. Arndt, Chem. Phys. Lett. 77, 239(1981).
13. S.M. George, A.L. Harris, M. Berg and C.B. Harris, in Picosecond Phenomena III, ed. by K.B. Eisenthal, R.M. Hochstrasser, W. Kaiser and A. Laubereau, Springer Ser. Chem. Phys. 23 (Springer-Verlag, Berlin, Heidelberg, New York, 1982) p. 196.
14. S.M. George and C.B. Harris, (submitted to Physical Review A).
15. W. Zinth, H.J. Polland, A. Laubereau and W. Kaiser Appl. Phys. B26, 77(1981).
16. A. Laubereau, G. Wochner and W. Kaiser Phy. Rev. 13A, 2212(1976); Opt. Commun. 17, 91(1976).

17. W. Zinth, A. Laubereau and W. Kaiser, Opt. Commun. 26, 457(1978).

18. D. Ben-Amotz, S.M. George and C.B. Harris, (to be published).

19. S.M. George and C.B. Harris, Rev. Sci. Instrum. 52, 852(1981).

20. S.J. Davis, J.E. Murray, D.C. Downs and W.H Lowdermilk Appl. Opt. 17, 3184(1978).

21. D.J. Bradley and G.H.C. New, Proc. IEEE 62, 313(1974).

22. D. von der Linde, O. Bernecker and W. Kaiser, Opt. Commun. 2, 149(1970).

23. J.A. Giordmaine, P.M. Rentzepis, S.L. Shapiro and K.W. Wecht Appl. Phys. Lett. 11, 216(1967).

24. J.L. Chao., Appl. Spect. 35, 281(1981).

25. The pulse widths Δt were determined using the expression $\Delta t=\beta\Delta$ where $\Delta\tau=2n\Delta z/c$ is the time width of the TPF autocorrelation width and β is the ratio of Δt and $\Delta\tau$ (Ref. 71). For Gaussian pulses, $\beta=1/(2)^{1/2}$ and for Lorentzian pulses $\beta=1/2$ (Ref. 71). Measured methanol refractive indices in the visible were extrapolated to give n=1.3235 at 1.06 μ.

26. D.J. Bradley, G.H.C. New and S.J. Caughey, Opt. Commun. 2, 41(1970).

27. D.J. Bradley and W. Sibbett, Opt. Commun. 9, 17(1973).

28. A. Penzkofer, Opto-Electron. 20, 87(1972).

29. The effect of Dye #5 as a saturable absorber was also studied. Under the same conditions, pulse shortening ratios of 0.84, 0.74 and 0.71 were observed for Dye #5 at optical densities of 1.0, 2.0 and 3.0, respectively. These smaller pulse shortening ratios were obtained at the cost of significant reduction of the pulse peak intensity.

30. Fresh spectrophotometric grade (99+%) acetonitrile was used from the bottle without further purification for each experimental run.

31. The Glan-laser double escape Q-switch polarizers were obtained from the Karl Lambrecht Corporation, 4204 N. Lincoln Avenue, Chicago, Illinois, 60618.

32. L.F. Mollenauer, C.D. Grandt, W.B. Grant and H. Panepucci, Rev. Sci. Instrum. 39, 1958(1968).

33. Shell Epon Resin 828 is made by the Shell Chemical Company. Versamid 140 polyamide resin is made by General Mills Chemicals, Inc.

34. The design for the low temperature cell was suggested by G. Williams, Univ. College of Wales, Aberystwyth, United Kingdom, and M.S. Beevers, Univ. of Aston, Birmingham, United Kingdom.

35. A.M. Phipps and D.N. Hume, J. Chem. Educ. 45, 664(1968). We used a mixture of approximately 0.6 volume fraction of o-xylene and 0.4 volume fraction of m-xylene.

36. W. Zinth, Appl. Phys. B26, 213(1981).

37. D.W. Oxtoby, J. Chem. Phys. 70, 2605(1979).

38. R.M. Lynden-Bell, Mol. Phys. 33, 907(1977).

39. J. Timmermans, Physico-Chemical Constants of Pure Organic Compounds (Elsecier, New York, 1950). p. 528.

40. A. Diamond, A. Fanelli and S. Petrucci, Inorg. Chem. 12, 611(1973).

41. Handbook of Chemistry and Physics, (Chemical Rubber Company, Cleveland).

42. A.Z. Francesconi, E.U. Franck and H. Lentz, Ber. Bunsenges. Phys. Chem. 79, 897(1975). Interpolated from liquid-vapor coexistence data at P=1 atmosphere.

43. K.A. Akhmetkarimov, I.I. Mai and Z.M. Muldakhmetov J. Gen. Chem. USSR 43, 460(1973).

44. F. Mato and J.L. Hernandez, Anal. Quim. 65, 9(1969).

45. W. Schindler and J. Jonas, J. Chem. Phys. 72, 5019(1980); J. Chem. Phys. 73, 3547(1980).

46. S.M. George and C.B. Harris, J. Chem. Phys. 77, 4781(1982).

47. R. Landau and A. Wurflinger, Ber. Bunsenges. Phys. Chem. 84, 895(1980).

48. Calculated isothermal compressibility values were obtained from A. Wurflinger, Dept. of Chemistry, Univ. of Bochum, 4630 Bochum 1, Federal Republic of Germany.

49. K. Arakawa and K. Kojima, Bull. Chem. Soc Jpn. 48, 26(1975).

50. Lange's Handbook of Chemistry, 12th Edition, ed. by J.A. Dean (McGraw-Hill, New York, 1979).

51. M.D. Zeidler, Ber. Bunsenges. Phys. Chem. 75, 769(1971).

52. A. Kratochwill, Ber. Bunsenges. Phys. Chem. 82, 783(1978).

53. A. Abragam, Principles of Nuclear Magnetism (Oxford Univ. Press, London, 1961) Chap.X. Sec.IV.

54. A. Fendt, S.F. Fischer and W. Kaiser, Chem. Phys. 57, 55(1981).

55. A. Laubereau, S.F. Fischer, K. Spanner and W. Kaiser, Chem. Phys. 31, 335(1978).

56. R. Zygan-Maus and S.F. Fischer, Chem. Phys. 41, 319(1979).

57. D.C. McKean, Spectrochim. Acta 29A, 1559(1973).

58. G. Herzberg, Molecular Spectra and Molecular Structure, Vol. II, (Van Nostrand Reinhold, New York, 1945) p. 332.

59. D.C. McKean, Spectrochim. Acta 30A, 1169(1974).

60. A.M. Saum, J. Polymer Science 42, 57(1960).

61. J.S. Rowlinson, Trans. Faraday Soc. 45, 974(1949).

62. J.D. Lambert, G.A.H. Roberts, J.S. Rowlinson and V.J. Wilkinson, Proc. Roy. Soc. (London) A196, 113(1949).

63. A. Loewenschuss and N. Yellin, Spectrochim. Acta 31A, 207(1975).

64. T.B. Freedman and E.R. Nixon, Spectrochim. Acta 28A, 1375(1972).

65. R.J. Jakobsen and J.W. Brasch, J. Am. Chem. Soc. 86, 3571(1964).

66. B.J. Bulkin, Helv. Chem. Acta 52, 1348(1969).

67. H. Saito, Y. Tanaka, S. Nagata and K. Nukada, Can. J. Chem. 51, 2118(1973).

68. C.S. Hsu and D. Chandler, Mol. Phys. 31, 215(1978).

69. A. Kratochwill, J.U. Weidner and H. Zimmerman, Ber. Bunsen. Gesellschaft 77, 408(1973).

70. H. Bertagnolli and M.D. Zeidler, Mol. Phys. 35, 177(1978).

71. E.P. Ippen and C.V. Shank in Ultrashort Light Pulses, Topics in Applied Physics, Vol 18, ed. by S.L. Shapiro (Springer-Verlag, Berlin, 1977).

Table Captions

TABLE 1. Experimental dephasing times, calculated homogeneous linewidths, isotropic Raman linewidths and inhomogeneous broadening linewidths for the symmetric CH_3-stretching vibration in acetonitrile versus temperature.

Figure Captions

FIG. 1. Schematic of the picosecond pulse generating system.

FIG. 2. Experimental setup for stimulated Stokes excitation and collinear Stokes probe scattering in a 10 cm Raman cell. Excitation Stokes and probe Stokes signals are separated because of their different polarizations and simultaneously detected using a two-dimensional OMA.

FIG. 3. Excitation laser pulse depletion examined by monitering the transmitted laser pulse energy with and without a 10 cm acetonitrile Raman cell. The approximate range of laser pulse energies used in the vibrational dephasing experiment is also shown.

FIG. 4. Vertical cross section of the temperature-controlled Raman cell equipped with the "gas window" design.

FIG. 5. Experimental data for the symmetric CH_3-stretching vibration in acetonitrile versus temperature. Coherently scattered Stokes signal as a function of probe delay at (a) -40° C and (c) -10° C. Isotropic Raman line shapes and homogeneous Lorentzian line shapes calculated from measured dephasing times at (b) -40° C and (d) -10° C.

FIG. 6. Experimental data for the symmetric CH_3-stretching vibration in acetonitrile versus temperature. Coherently scattered Stokes signal as a function of probe delay at (a) 18° C and (c) 70° C. Isotropic Raman line shapes and homogeneous Lorentzian line shapes calculated from measured dephasing times at (b) 18° C and (d) 70° C.

FIG. 7. Experimental dephasing times from individual measurements versus temperature. The measurements are numbered according to the sequence in which they were performed.

FIG. 8. Temeperature dependent vibrational linewidth broadening in acetonitrile. (a) Correlation of experimentally determined homogeneous linewidths and predicted homogeneous linewidths normalized at 18° C. (b) Correlation of experimentally determined inhomogeneous linewidths and absolute inhomogeneous linewidths predicted by the Schweizer-Chandler theory using three representative N values.

FIG. 9. Isothermal compressibility versus temperature in acetonitrile. The filled-in circles are experimental values from A. Wurflinger (Refs. 47,48). The line shows the fit of a hard sphere model (Ref. 49) to the experimental values.

FIG. 10. Translational self-diffusion constant versus temperature in acetonitrile. The filled-in circles are experimental values from M.D. Zeidler (Ref. 51). The open triangles are experimental values from A. Kratochwill (Ref. 52).

FIG. 11. Correlation between experimentally measured dephasing times, $T_2/2$, and the predicted $T_2/2$ times calculated using Eqn. (4) which includes diffusional site exchange. The predicted $T_2/2$ dephasing times were fit to the data using τ=4 psec at 70° C. The pure dephasing times, $T_2^*/2$, from the hydrodynamic dephasing theory are also shown.

TABLE 1

Temperature (°C)	Average Experimental $T_2/2$ (ps)	Calculated Homogeneous $\Delta\omega$ (cm^{-1})	Isotropic Raman $\Delta\omega$ (cm^{-1})	Gaussian Inhomogeneous $\Delta\omega$ (cm^{-1})
70	1.4	3.8	6.5	4.1
45	2.1	2.5	6.5	5.1
18	2.3	2.3	6.5	5.2
-10	1.6	3.4	6.6	4.5
-45	1.0	5.2	6.8	3.3

38

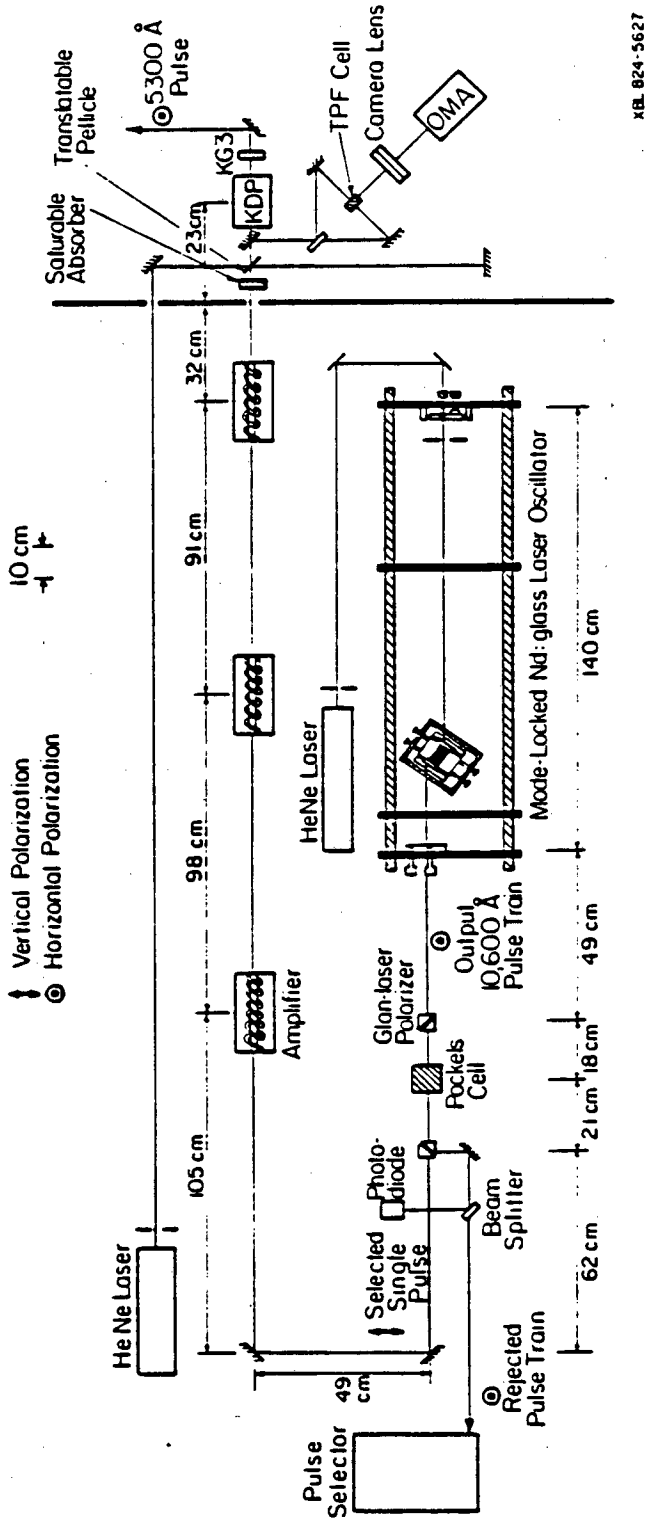

FIG. 1

George, Harris
Berg & Harris

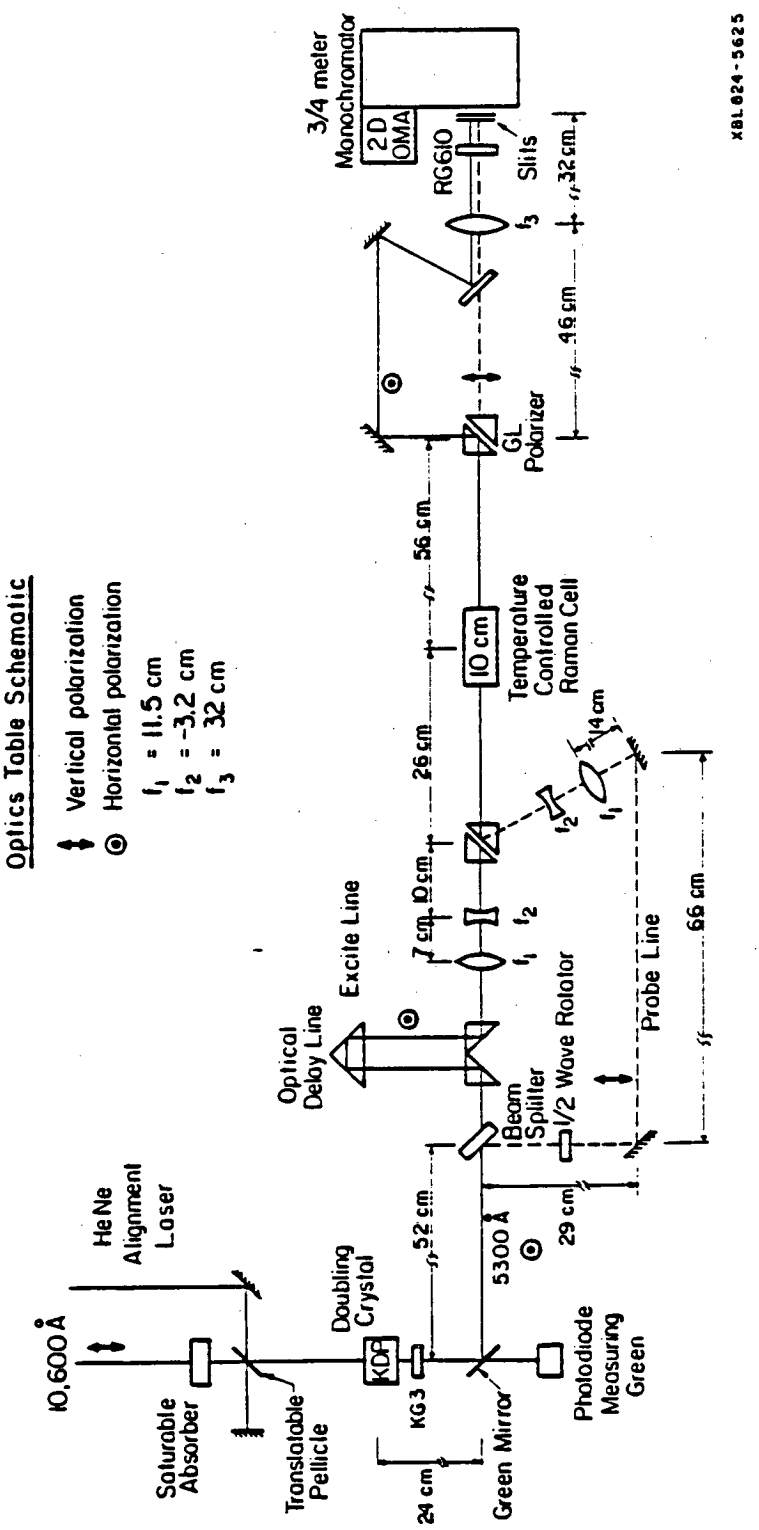

FIG. 2

George, Harris
Berg & Harris

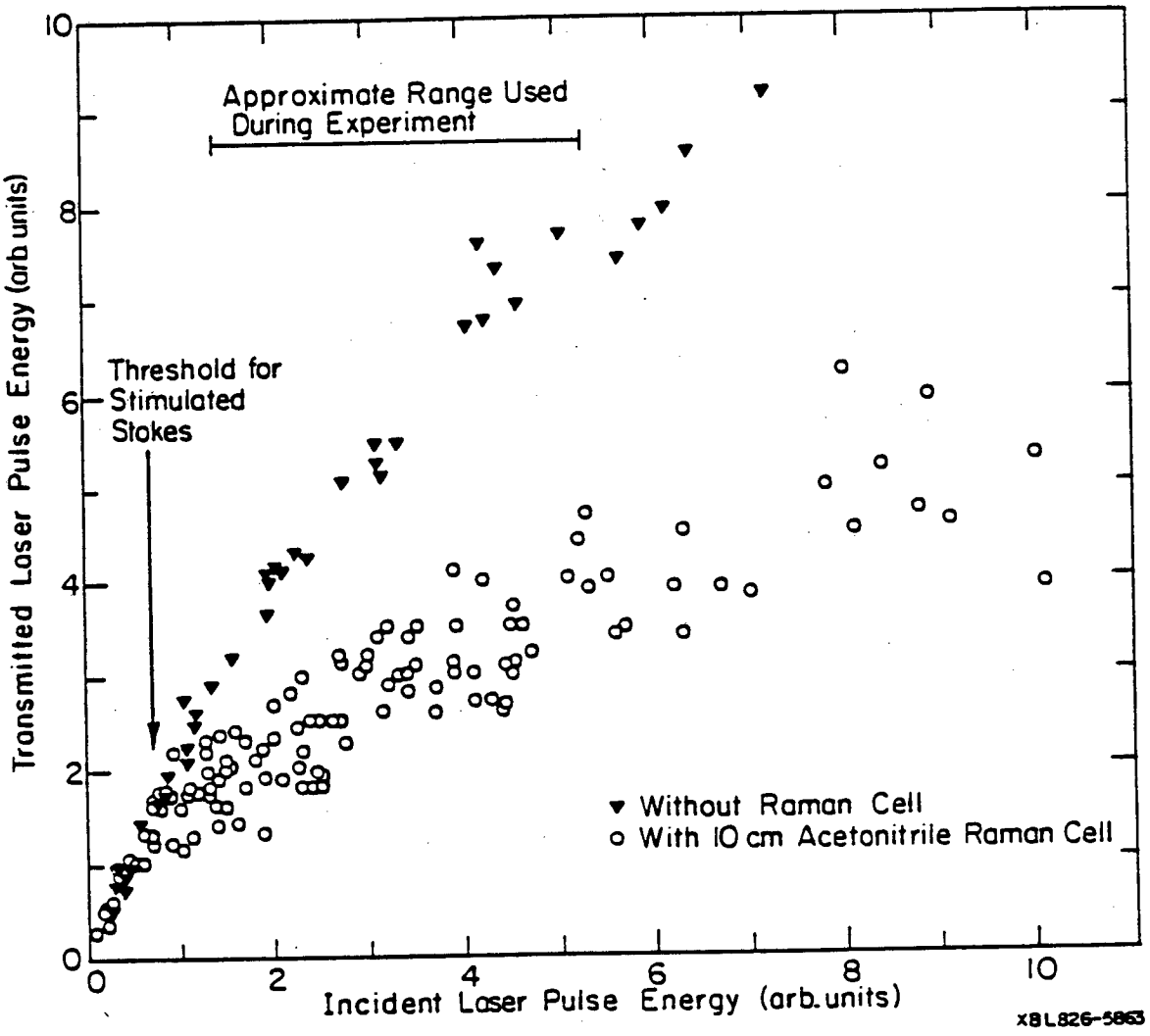

FIG. 3

George, Harris, Berg & Harris

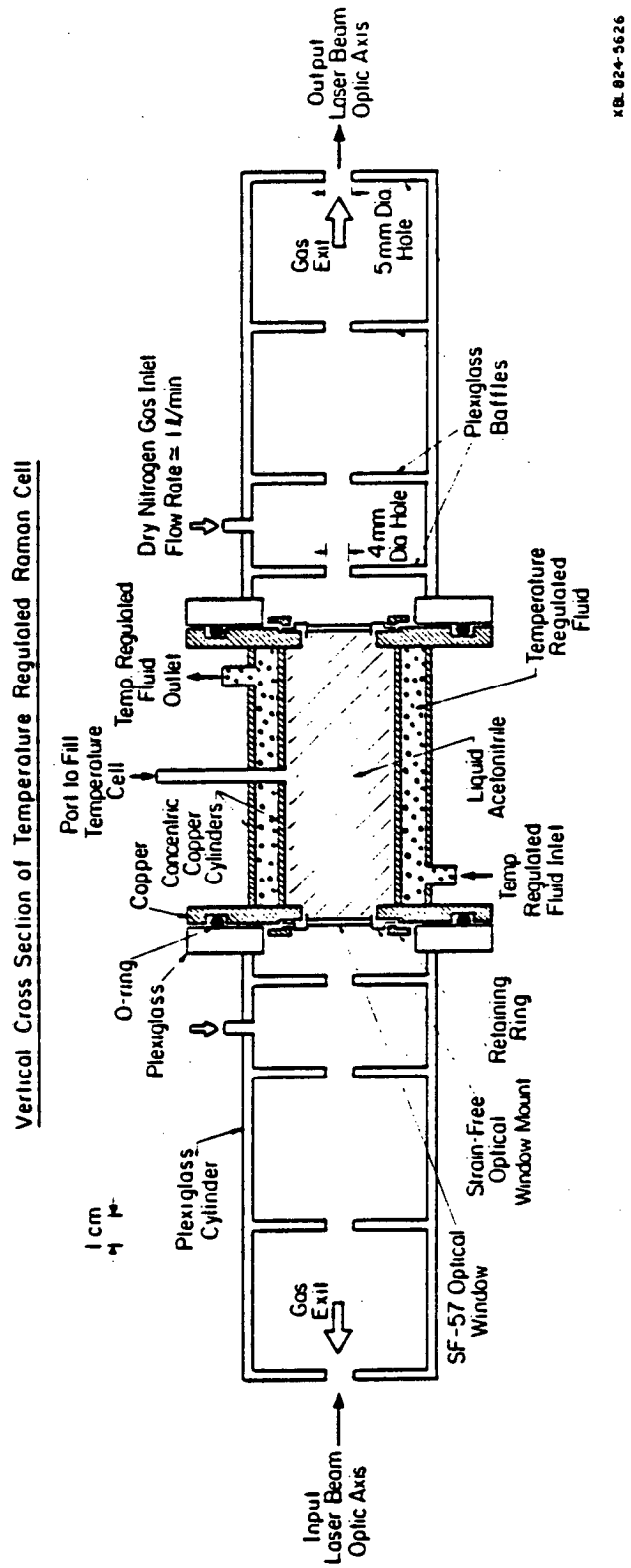

FIG. 4

George, Harris, Berg & Harris

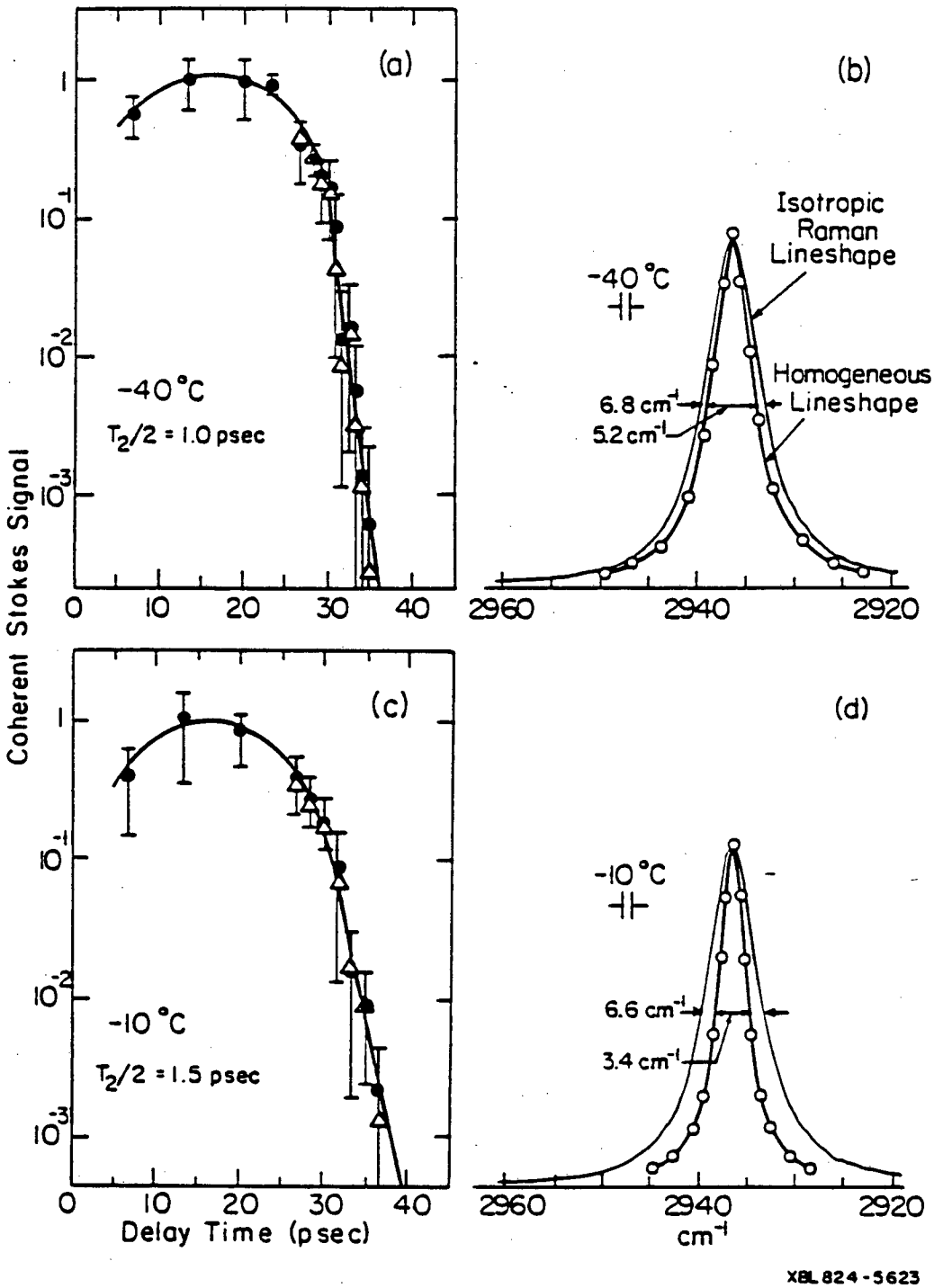

FIG. 5

George, Harris
Berg & Harris

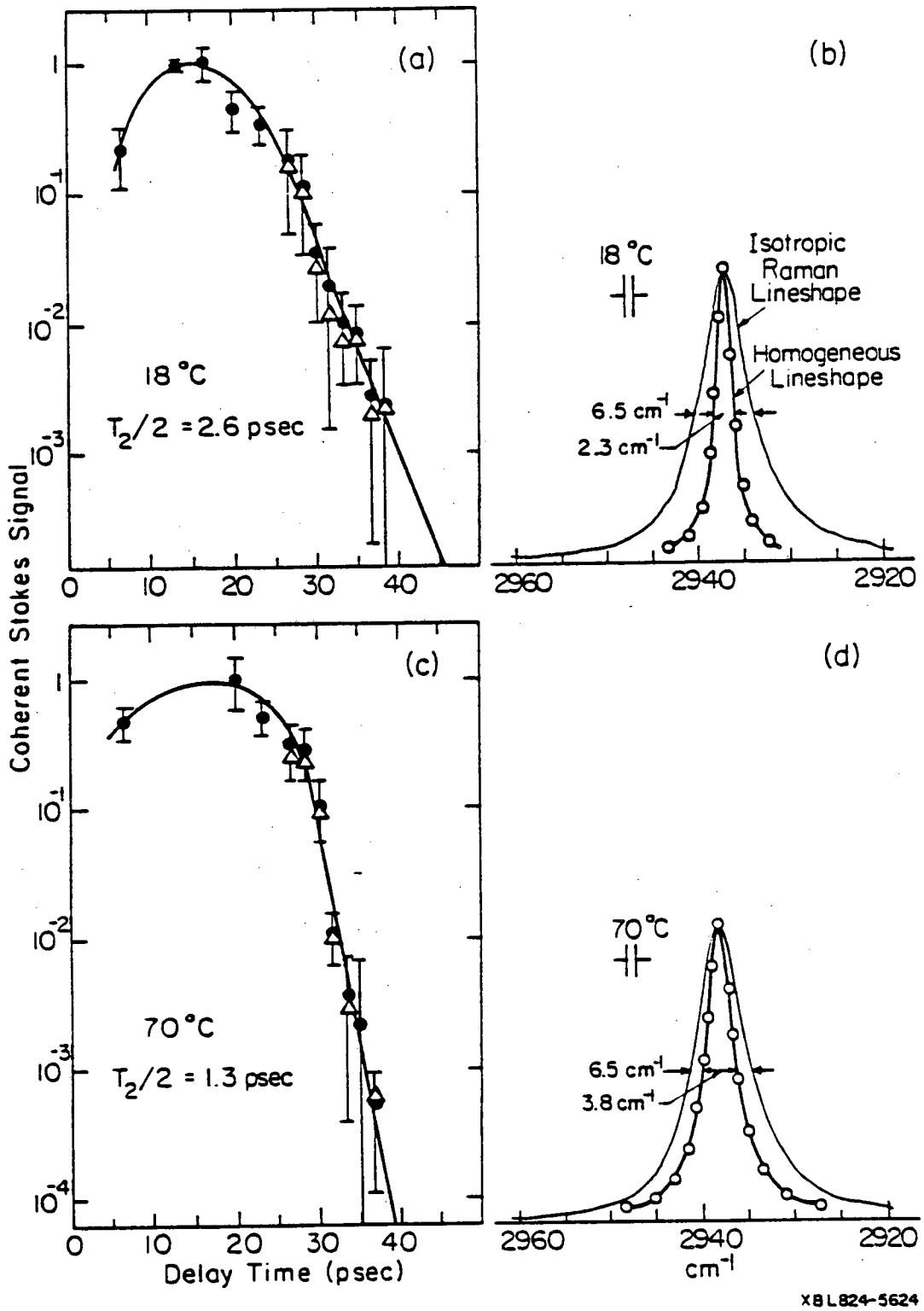

FIG. 6

George, Harris
Bera & Harris

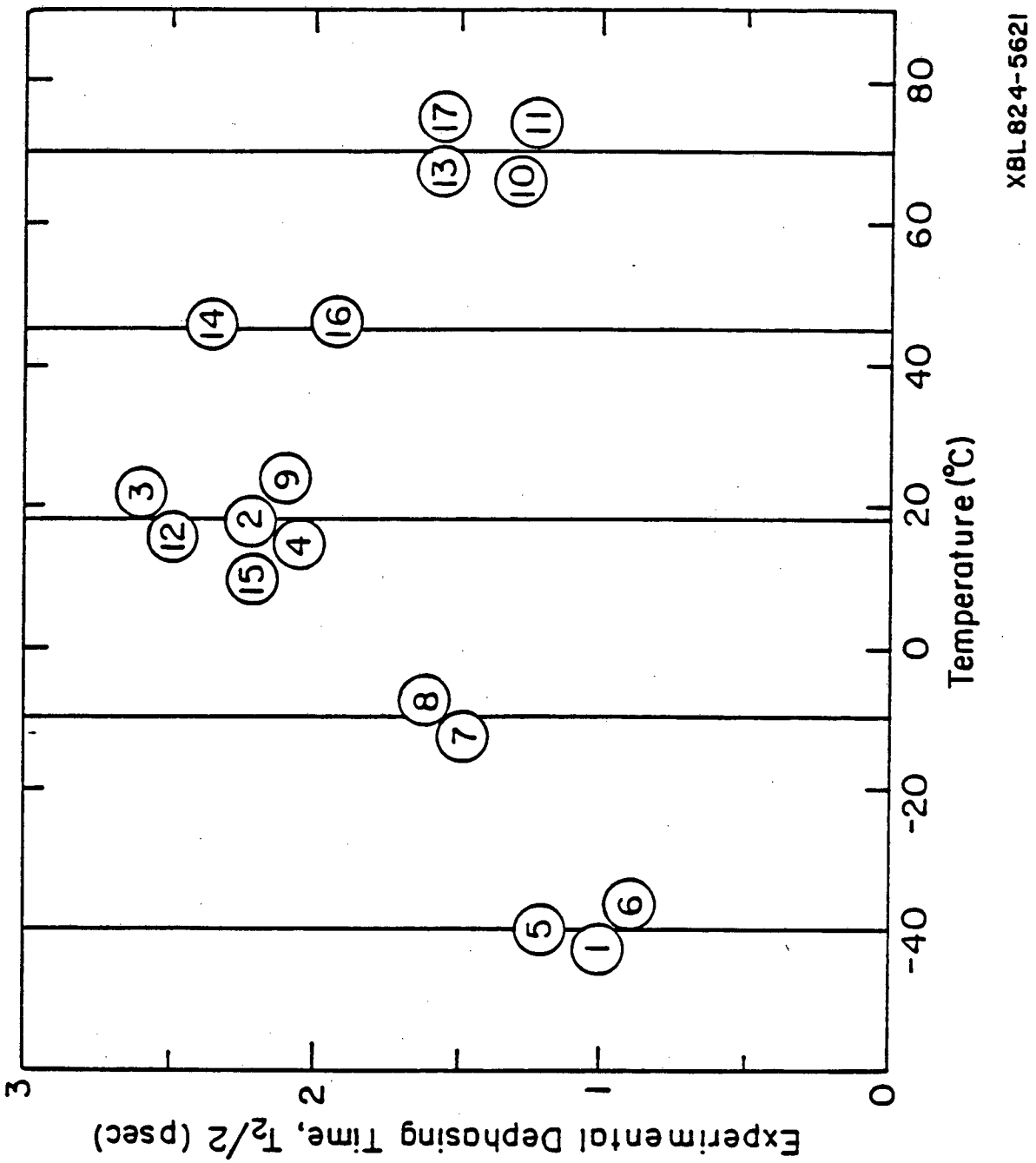

XBL824-5621

FIG. 7

George, Harris, Berg & Harris

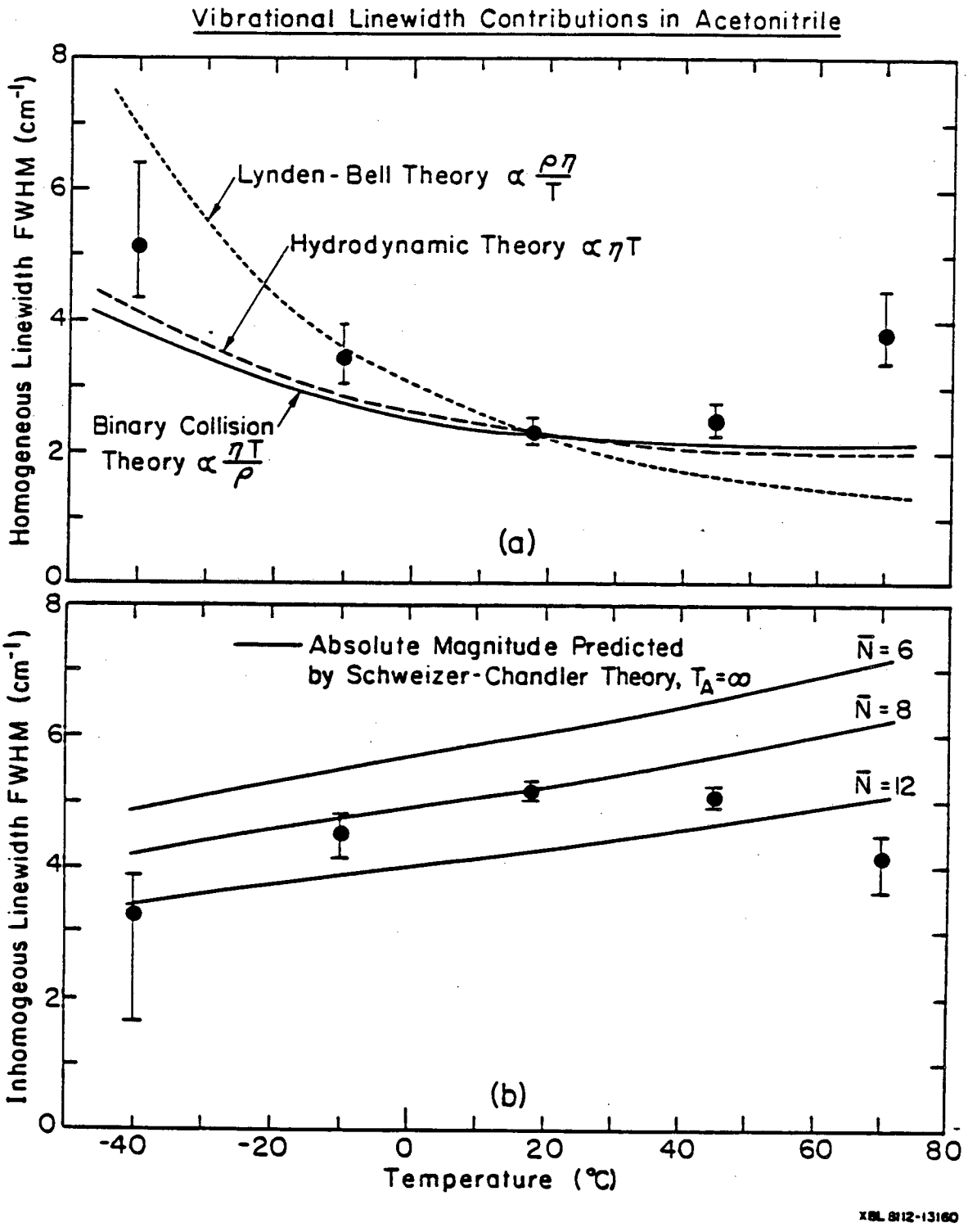

FIG. 8

George, Harris, Berg & Harris

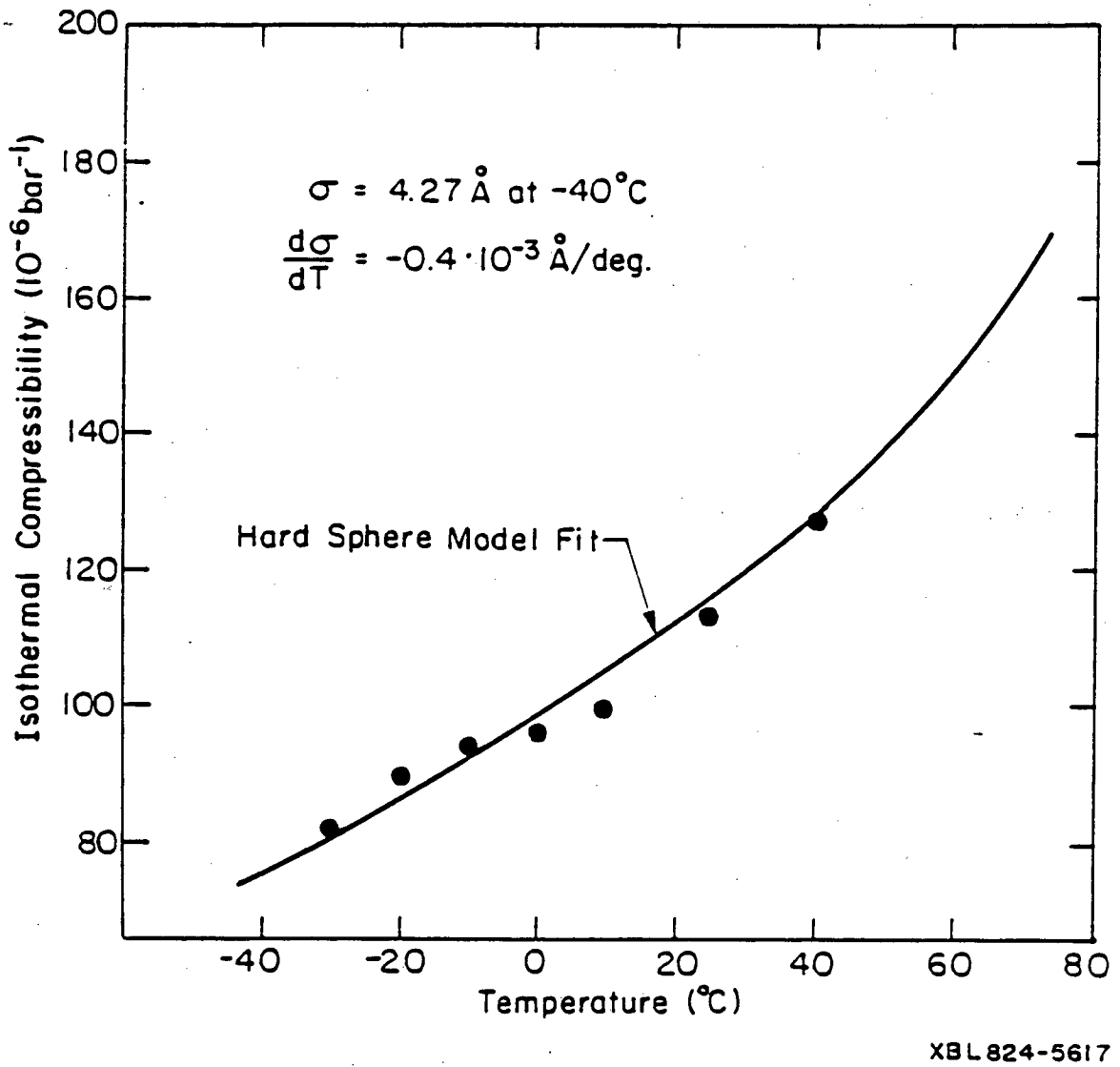

FIG. 9

George, Harris, Berg & Harris

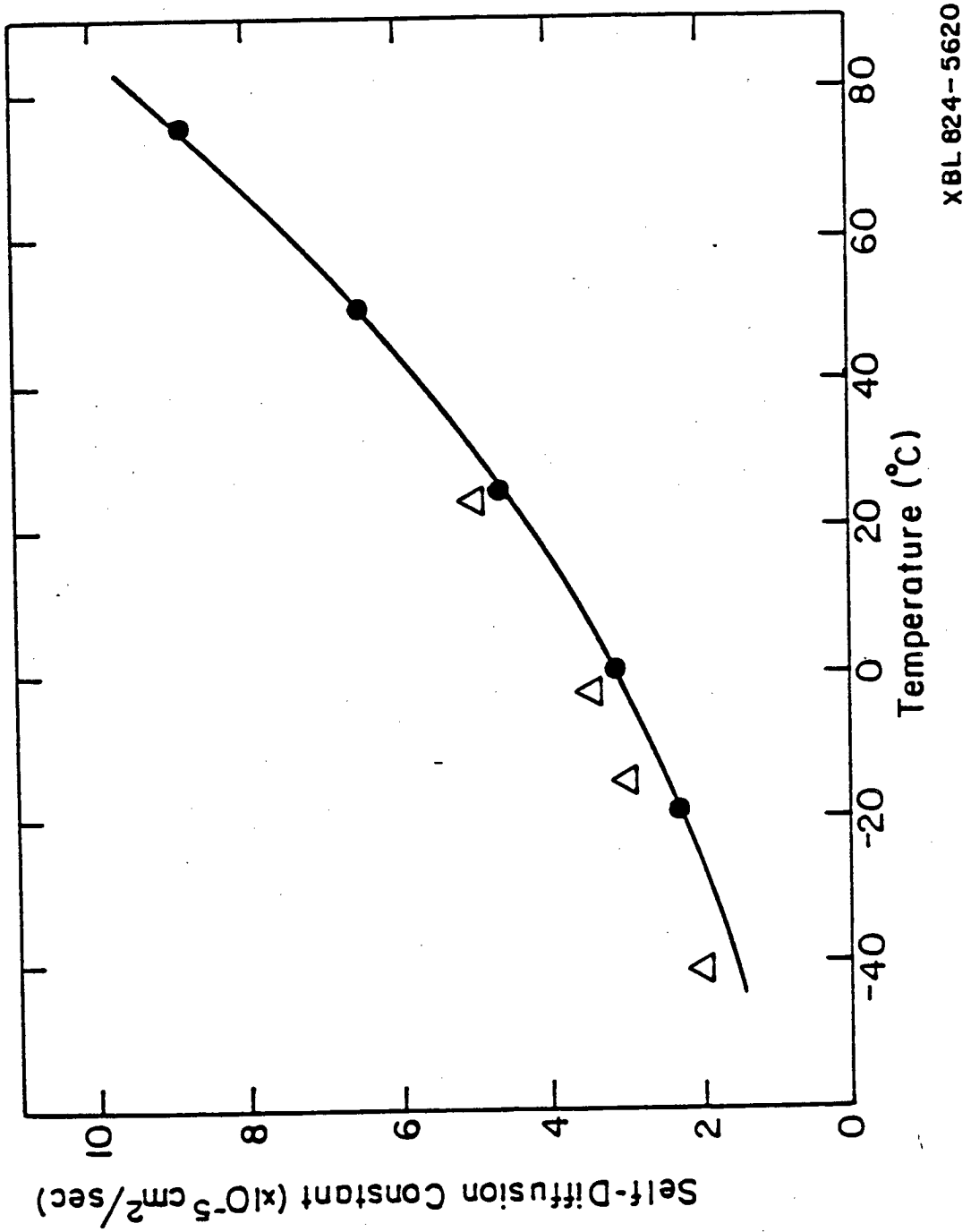

FIG. 10

George, Harris,
Berg & Harris

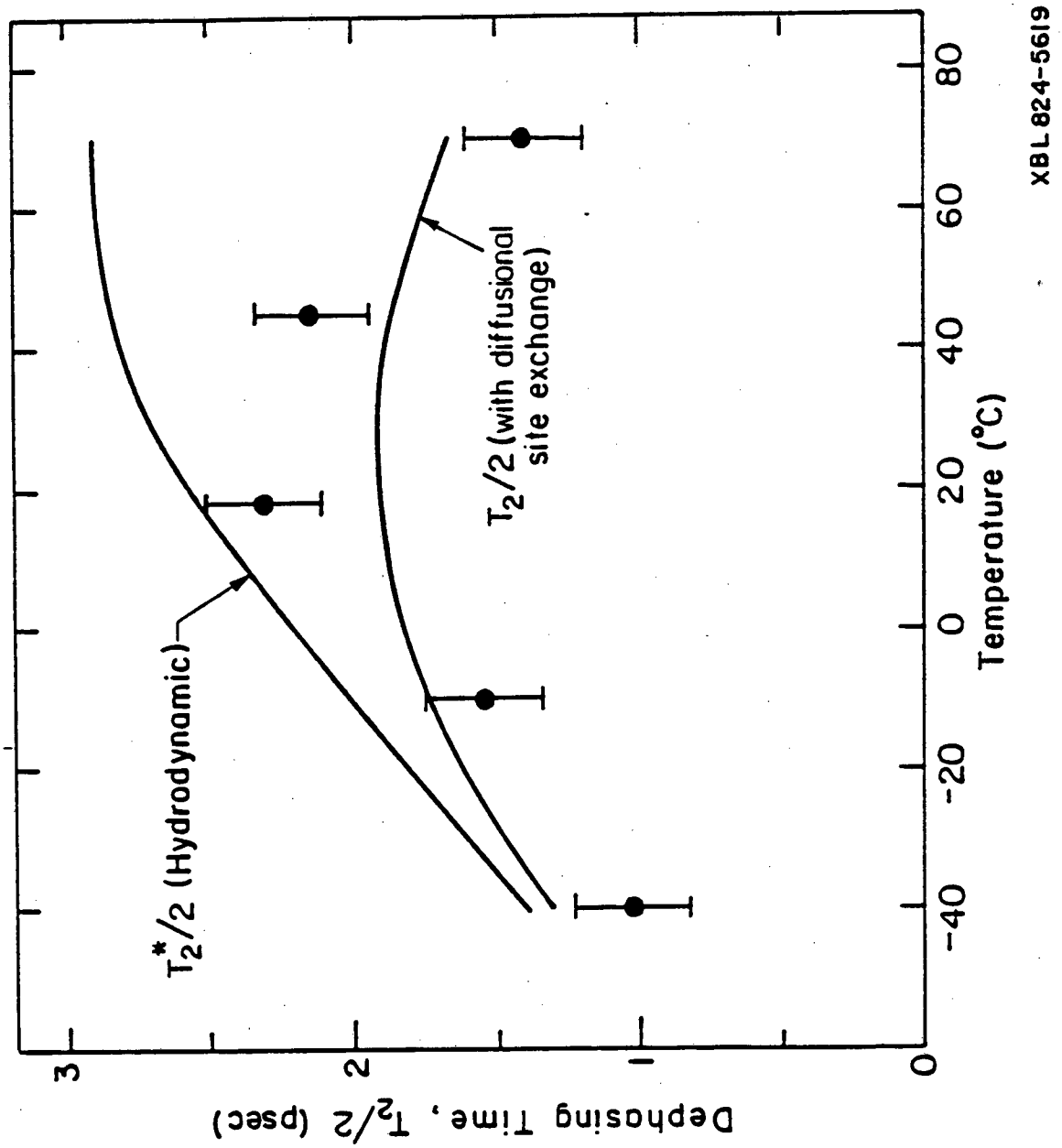

FIG. 11

George, Harris, Berg & Harris

TECHNICAL INFORMATION DEPARTMENT
LAWRENCE BERKELEY LABORATORY
UNIVERSITY OF CALIFORNIA
BERKELEY, CALIFORNIA 94720